$CaIrO_3$: A Spin-Orbit Mott Insulator Beyond the $j_{\text{eff}} = 1/2$ Ground State

M. Moretti Sala,[1,*] K. Ohgushi,[2] A. Al-Zein,[1] Y. Hirata,[2] G. Monaco,[3,1] and M. Krisch[1]
[1]European Synchrotron Radiation Facility, BP 220, F-38043 Grenoble Cedex, France
[2]Institute for Solid State Physics, University of Tokyo, Kashiwa, Chiba 277-8581, Japan
[3]Dipartimento di Fisica, Università di Trento, via Sommarive 14, 38123 Povo (TN), Italy
(Received 27 January 2014; published 30 April 2014)

In $CaIrO_3$, electronic correlation, spin-orbit coupling, and tetragonal crystal field splitting are predicted to be of comparable strength. However, the nature of its ground state is still an object of debate, with contradictory experimental and theoretical results. We probe the ground state of $CaIrO_3$ and assess the effective tetragonal crystal field splitting and spin-orbit coupling at play in this system by means of resonant inelastic x-ray scattering. We conclude that insulating $CaIrO_3$ is *not* a $j_{\text{eff}} = 1/2$ iridate and discuss the consequences of our finding to the interpretation of previous experiments. In particular, we clarify how the Mott insulating state in iridates can be readily extended beyond the $j_{\text{eff}} = 1/2$ ground state.

DOI: 10.1103/PhysRevLett.112.176402 PACS numbers: 71.70.Ej, 71.27.+a, 78.70.En

Spin-orbit coupling is the main ingredient for $5d$ transition metal oxides to form novel electronic states of matter, such as the recently discovered Mott insulating state in Sr_2IrO_4 [1–3]. This insulating behavior is unexpected in iridate perovskites because, for a half-filled shell with spatially extended orbitals, electronic correlation was thought to be negligible. Instead, the role of electronic correlation is enhanced here by spin-orbit coupling through the formation of the so-called $j_{\text{eff}} = 1/2$ ground state. Its realization arises from the interaction of strong spin-orbit coupling ($\zeta \sim 0.5$ eV) and a cubic crystal field ($10\text{Dq} \sim 3$ eV), and is perturbed by short- and long-ranged anisotropies which could cause departures from the $j_{\text{eff}} = 1/2$ ground state [4–7]. A small, but sizable tetragonal contribution $|\Delta| \sim 0.01$ eV to the cubic crystal field 10Dq was detected in both Sr_2IrO_4 [6] and Ba_2IrO_4 [7], with opposite signs, in agreement with recent theoretical calculations [5]. In these cases, however, $|\Delta| \ll \zeta \ll 10\text{Dq}$ and the $j_{\text{eff}} = 1/2$ ground state in Sr_2IrO_4 and Ba_2IrO_4 is not in doubt. Structural distortions are instead more pronounced in the insulating post-perovskite $CaIrO_3$ [8]; thus, the cubic symmetry of the crystal field is expected to be drastically lowered and the $j_{\text{eff}} = 1/2$ ground state to be severely altered. The robustness of the $j_{\text{eff}} = 1/2$ ground state against structural distortions, in particular octahedral rotations and elongations, as well as chemical substitution has been mostly tested by means of resonant x-ray magnetic scattering (RMXS), on the basis of the nearly vanishing intensity at the L_2 absorption edge [3]. Following this criterion, a number of "$j_{\text{eff}} = 1/2$ iridates" have been identified [9–13], including $CaIrO_3$ [14]. However, this interpretation has been widely controversial [15–17]. Indeed, a unified picture has not been reached yet: the interpretation of RMXS results [14] is only partially compatible with LDA + SO + U calculations [18] and has been contradicted by *ab initio* quantum chemistry calculations [19]. The former predicted values of the spin and orbital contribution to the magnetic moment are different from what was expected for the $j_{\text{eff}} = 1/2$ state, the latter a large splitting of the t_{2g} states that gives rise to a strongly unbalanced occupation of the xy, yz, and zx orbitals (while for the $j_{\text{eff}} = 1/2$ ground state the three orbitals should contribute with an equal weight of $1/3$). Nevertheless, a consensus is reached on the magnetic interactions, with a strong antiferromagnetic coupling along the c axis and a weak ferromagnetic one along the a axis, which stabilize canted long range antiferromagnetism [18,20] and characterize $CaIrO_3$ as a quasi-one-dimensional antiferromagnet [19].

In this Letter, we use resonant inelastic x-ray scattering (RIXS) at the Ir L_3 edge to solve the puzzle of the ground state in $CaIrO_3$. RIXS is a powerful technique for the study of correlated electron systems [21]. Recently, it was applied to the investigation of magnetic excitations in correlated iridium oxides. Following the initial theoretical suggestion of Ament *et al.* [22], it was demonstrated that magnon dispersion could be studied in Sr_2IrO_4 [23,24] and $Sr_3Ir_2O_7$ [25]. In the present work, we focus on the inelastic response of $CaIrO_3$ in the energy range relevant to spin-orbital excitations [23,26–28] and we determine the effective tetragonal crystal field and spin-orbit coupling acting on t_{2g} levels by comparing the results to a single-ion model [17,22,27]. We obtain $\zeta = 0.52$ and $\Delta = -0.71$ eV and therefore conclude that the departure of $CaIrO_3$ from the $j_{\text{eff}} = 1/2$ state is unambiguous, in agreement with *ab initio* calculations [19].

RIXS measurements were performed at the new inelastic x-ray scattering beam line of ESRF (ID20-UPBL06). Two different setups were used in order to optimize the flux and energy resolution of the beam line, providing bandwidths of 25 and 350 meV, respectively (Supplemental Material [29]). A single crystal of $CaIrO_3$ was grown by the flux

method as in Ref. [14]. $CaIrO_3$ has a post-perovskite structure, composed of edge-sharing (corner-sharing) IrO_6 octahedra along the a axis (c axis), in which each octahedron is compressed along the corner-sharing O direction (the local z direction) with a bond length ratio of 0.97. Because of the alternating rotation of the octahedra around the a axis, the local z axis and the crystallographic c axis form an angle of $\pm 23°$, thus forming a zigzag chain of Ir-O-Ir bonds. $CaIrO_3$ is an insulator and undergoes a transition to a canted antiferromagnet at $T_N = 115$ K [20], in which the strong spin-orbit coupling stabilizes a striped-type magnetic order (magnetic moments are aligned parallel along a and mostly antiparallel along c, with a small canting in the direction of the b axis) [14]. Throughout the experiment, the sample was kept at a temperature of 15 K.

Figure 1 shows a low energy-resolution RIXS map of $CaIrO_3$, in which the incident photon energy is scanned across the L_3 absorption edge and a series of spectra are recorded for up to 12 eV of energy loss. An elastic line, magnetic excitations, and possibly phonons are found close to the zero energy loss line. At increasing energy losses, we assign features to intra-t_{2g} ($t_{2g}^5 \rightarrow t_{2g}^5$), t_{2g}-to-e_g ($t_{2g}^5 \rightarrow t_{2g}^4 e_g^1$), and charge-transfer excitations (as indicated in the figure), following previous RIXS studies [32]. In this work, we concentrate on intra-t_{2g} excitations only. Their intensity (including that of the elastic line and magnetic excitations) is enhanced for incident photon energies about 3 eV below the main absorption peak. This is a common feature of several iridium oxides, which was observed in both RMXS and RIXS experiments [9,26]. It can be understood by considering the electronic structure of an Ir^{4+} ion in a large cubic crystal field: with five electrons filling the $5d$ states, e_g states are empty and one hole is left in the t_{2g} states. The maximum of the absorption line (11.219 keV) corresponds to the transition of an electron into the $5d$ e_g state, while the contribution of the t_{2g} states is minor, as it scales with the number of unoccupied final states. On the other hand, it is reasonable to assume that intra-t_{2g} excitations are more effectively probed when a $2p_{3/2}$ electron is directly promoted in the $5d$ t_{2g} state, i.e., for incident photon energies tuned at $\sim$10Dq below the main absorption line (11.216 keV).

For the high resolution measurements, we fixed the incident photon energy at 11.216 keV to enhance t_{2g} excitations. A representative spectrum is shown in Fig. 2. We do not discuss here the low energy features. The 0.3–1.6 eV energy range is dominated by two intense broad features (B and C) and a weak, energy-resolution limited peak (A), similar to the excitation spectrum of Na_2IrO_3 and Li_2IrO_3 [28,33]. The assignment of features B and C to local excitations across crystal field split states [28] was initially debated [34], but then supported by recent calculations [35]. We therefore assign features B and C of Fig. 2 in analogy to the case of Na_2IrO_3 and Li_2IrO_3. The assignment of features B and C is further strengthened by *ab initio* calculations for $CaIrO_3$ predicting a splitting of the $j_{\text{eff}} = 3/2$ states by

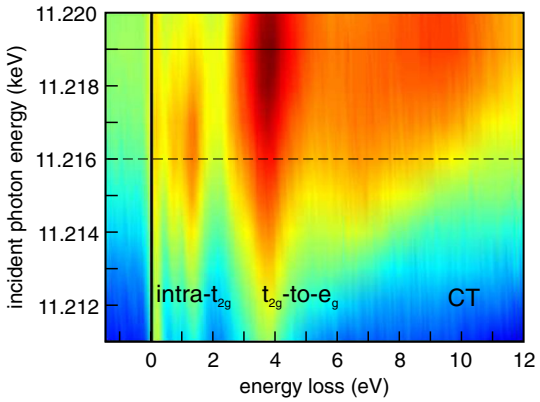

FIG. 1 (color online). RIXS color map of $CaIrO_3$. The continuous vertical line corresponds to the maximum of the absorption profile at 11.219 keV. The dashed vertical line, instead, corresponds to the incident photon energy used for the high energy-resolution RIXS spectrum of Fig. 2 (11.216 keV).

0.6–0.7 eV [19], in agreement with the energy difference of about 0.6 eV for features B and C found in our experiment.

In the following we discuss the spin-orbit excitations (features B and C in Fig. 2) in more detail. Although of mostly local origin, it should be mentioned that they show a weak, but non-negligible dispersion versus momentum transfer, in the order of 0.05 eV, indicating that they retain some nonlocal character. In the present work, however, we aim at determining the size of the effective tetragonal crystal field splitting and spin-orbit coupling in $CaIrO_3$ and the fine details of the band structure will therefore be neglected. The *effective* parameters Δ and ζ will then include any kind of renormalization due to nonlocal effects. A dedicated study of the transferred momentum dependence of such excitations is, however, desirable.

The spectra were fitted to three Pearson functions: feature A turns out to be energy-resolution limited, at an energy of about 0.42 eV, which is very similar to the value reported for Na_2IrO_3 and Li_2IrO_3 [28]. Features B and C are centered at 0.65 and 1.22 eV, respectively. In order to better understand the nature of these excitations, and to assess the effective tetragonal crystal field splitting and spin-orbit coupling in $CaIrO_3$, we adopt a single-ion model [7,14,17,22,26,27]. The weak momentum transfer dependence of these excitations suggests a dominant intrasite character, for which a local model is justified. Since 10Dq is sufficiently large (10Dq $\sim$ 3 eV), $5d$ e_g states are neglected and the interacting Hamiltonian for one *hole* in the $5d$ t_{2g} states is then written as

$$\mathcal{H} = \zeta \mathbf{L} \cdot \mathbf{S} - \Delta L_z^2, \tag{1}$$

in which tetragonal crystal field splitting ($\Delta < 0$ for compressed octahedra) and spin-orbit coupling are treated on equal footing. For $\Delta = 0$, the ground state is represented by

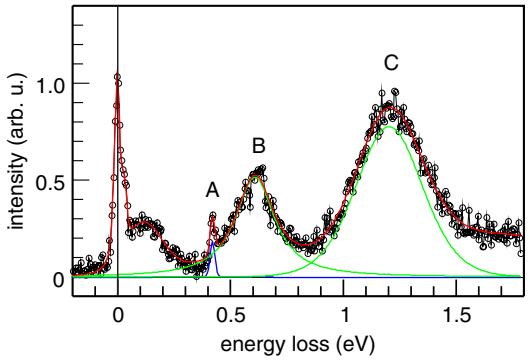

FIG. 2 (color online). RIXS spectrum of $CaIrO_3$ at a selected momentum transfer $\mathbf{Q} = \mathbf{k}_o - \mathbf{k}_i = (-1.2, 1.2, 5.9) - (-2.2, -0.8, -4.1) = (1, 2, 10)$ reciprocal lattice units and incoming π-polarized radiation. Continuous lines are fit to the experimental data.

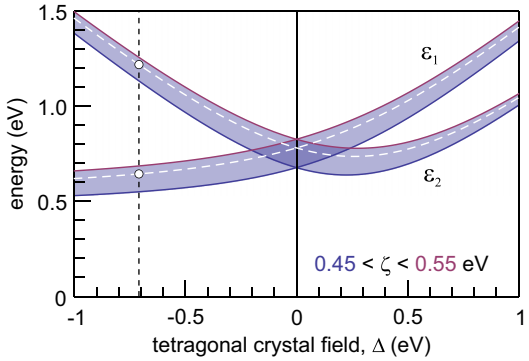

FIG. 3 (color online). Energy diagram of spin-orbit excitations calculated according to Eqs. (2) and (3) as a function of Δ for $0.45 < \zeta < 0.55$ eV. White dashed lines correspond to the estimated value of $\zeta = 0.52$ eV, while the white dots correspond to the actual value of the spin-orbit excitations in $CaIrO_3$.

the $|j_{\text{eff}} = 1/2\rangle$ doublet and the excited states by the $|j_{\text{eff}} = 3/2\rangle$ quadruplet. For arbitrary values of ζ and Δ, the eigenstates of $\mathcal{H}$ are three nondegenerate Kramers doublets, which we generically label $|0, \pm\rangle$, $|1, \pm\rangle$, and $|2, \pm\rangle$ ($|0, \pm\rangle$ being the ground state wave function). The corresponding eigenvalues, E_0, E_1, and E_2, are reported, for example, in Ref. [17]. Here we are interested in transitions from the $|0, \pm\rangle$ ground state to the $|1, \pm\rangle$ and $|2, \pm\rangle$ excited states. The corresponding energies, relative to the ground state, are given by

$$\varepsilon_1 = E_1 - E_0 = \frac{\zeta}{4}[3 + \delta + \sqrt{9 + \delta(\delta - 2)}], \quad (2)$$

$$\varepsilon_2 = E_2 - E_0 = \frac{\zeta}{2}\sqrt{9 + \delta(\delta - 2)}, \quad (3)$$

where $\delta = 2\Delta/\zeta$. These are reported in Fig. 3 as a function of Δ for $0.45 < \zeta < 0.55$ eV. For $\Delta = 0$, $\varepsilon_1 = \varepsilon_2 = 3\zeta/2$ as the $|1, \pm\rangle$ and $|2, \pm\rangle$ states merge into the $|j_{\text{eff}} = 3/2\rangle$ quadruplet when the $j_{\text{eff}} = 1/2$ ground state is realized. In general, however, the energy of the two RIXS excitations is a function of both Δ and ζ.

In our case, the only solution with physical meaning is found by imposing $\varepsilon_1 = 0.65$ and $\varepsilon_2 = 1.22$ eV (white dots in the diagram of Fig. 3), from which one obtains $\zeta = 0.52$ and $\Delta = -0.71$ eV and the expression for the ground state wave function $|0, \pm\rangle = \mp 0.32|xy, \mp\rangle + 0.67(|yz, \pm\rangle \mp \imath|zx, \pm\rangle)$. The value of ζ compares favorably with previous estimates in other iridium oxides [7,12,26,28], and in particular to the recently calculated value of 0.47 eV by Bogdanov *et al.* [19] for the specific case of $CaIrO_3$. The sign of Δ is consistent with structural studies reporting a compression of the IrO_6 octahedra [8], while its magnitude implies a minor contribution of the xy orbital to the ground state wave function (only $0.32^2 \approx 10\%$), in agreement with *ab initio* quantum chemistry calculations which predict a splitting of t_{2g} states in the absence of spin-orbit coupling in the order of 0.63–0.76 [19]. Noteworthy, $|\Delta|$ is more than 1 order of magnitude larger than that of the prototypical $j_{\text{eff}} = 1/2$ compounds, Sr_2IrO_4 ($|\Delta| = 0.01$ eV) [6] and Ba_2IrO_4 ($|\Delta| = 0.05$ eV) [17], and significantly larger than that due to trigonal distortions in Na_2IrO_3 and Li_2IrO_3 ($|\Delta| < 0.18$ eV) [28], and $Eu_2Ir_2O_7$ ($|\Delta| = 0.54$ eV) and $Y_2Ir_2O_7$ ($|\Delta| = 0.59$ eV) [27]. Therefore, $|\Delta| > \zeta$ and we can safely state that $CaIrO_3$ is *not* a $j_{\text{eff}} = 1/2$ iridate, with a dominant $(|yz, \pm\rangle \mp \imath|zx, \pm\rangle)/\sqrt{2}$ character of the ground state wave function.

We now discuss the size and direction of the magnetic moments in comparison to existing experimental results and the sign of magnetic interactions. The size of the magnetic moment is a function of both ζ and Δ [17]: with the above determined values, the magnetic moment turns out to be $1.7\mu_B$ in $CaIrO_3$, i.e., larger than $1\mu_B$ expected for a perfectly localized $j_{\text{eff}} = 1/2$ state. Following the interpretation of magnetization data of Ref. [14], we conclude that the magnetic moments in $CaIrO_3$ are canted along the b axis, with a canting angle of $\sim 2°$, i.e., about 21° away from the local z axis of the IrO_6 octahedra. It should be noted here that the discrepancy between RMXS and RIXS results is reconciled in view of their nontrivial dependence on the magnetic moment direction [17]. Indeed, considering the actual value of Δ and ζ, and the direction of the magnetic moments, one obtains a Ir L_2/L_3 RMXS intensity ratio of 0.1%, which is below the detectability limit of 0.3% reported in the experiment [14] (it would be 24% in the case of magnetic moments aligned along the local z axis). Magnetic interactions giving rise to the stripe-type canted antiferromagnetism of $CaIrO_3$ discussed above were explained in the framework of an ideal $j_{\text{eff}} = 1/2$ state [14], for which theoretical arguments [36] predict antiferromagnetic (ferromagnetic) coupling along the corner-shared (edge-shared) bonds. However, as long as the occupancy of the yz and zx orbitals is identical and their

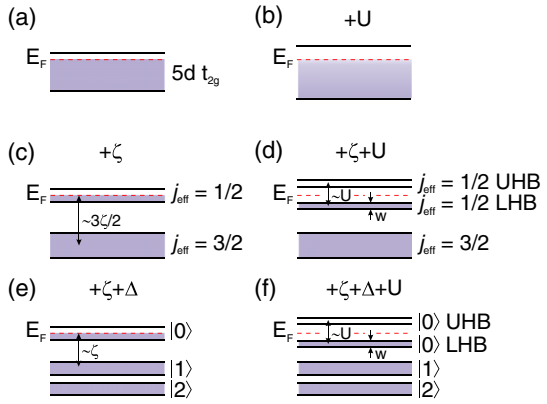

FIG. 4 (color online). Schematic representations of the band structure in iridates with $5d^5$ configurations in the absence of perturbations (a), with spin-orbit coupling (c), and spin-orbit coupling plus tetragonal crystal field splitting (e). Panels (b), (d), and (f) correspond to panels (a), (c) and (e), respectively, when the Hubbard term U is taken into account.

phase relation preserved, the same theoretical arguments apply and the sign of the magnetic interactions remains unchanged.

We are now in the position to discuss the transport properties of iridates and their connection to the $j_{\mathrm{eff}} = 1/2$ ground state. The latter was originally invoked to explain the insulating behavior of Sr_2IrO_4 and readily applied to other "$j_{\mathrm{eff}} = 1/2$" compounds. In Fig. 4 we explain and extend the concept of a spin-orbit Mott insulator beyond the specific case of $j_{\mathrm{eff}} = 1/2$ iridates. One has to consider the $5d$ t_{2g} states, whose bandwidth in the absence of perturbations would be too large for a reasonable Hubbard energy U to open a gap; rather, the density of states at the Fermi energy would be only slightly reduced, as in Fig. 4(b). Crucially, spin-orbit coupling in the absence of a tetragonal crystal field splits the otherwise degenerate t_{2g} states and a half-filled $j_{\mathrm{eff}} = 1/2$ band is isolated, with a much reduced bandwidth (w) compared to the original one. As $U > w$, lower and upper Hubbard bands are created, thus turning the system into an insulator [Fig. 4(d)] [1]. In $CaIrO_3$, however, the large tetragonal crystal field degrades the $|j_{\mathrm{eff}} = 1/2\rangle$ ground state into the generic $|0\rangle$. Nevertheless, the smallest splitting between the $j_{\mathrm{eff}} = 1/2$- and $j_{\mathrm{eff}} = 3/2$-derived bands is ζ (ε_1 in the limit $\Delta \to -\infty$), i.e., only a factor $3/2$ smaller than that in the pure $j_{\mathrm{eff}} = 1/2$ ground state. Therefore, for $U > w$, lower Hubbard bands and upper Hubbard bands are formed and the system retains its insulating character, although the ground state wave function differs significantly from $|j_{\mathrm{eff}} = 1/2\rangle$. A rough estimate of U in $CaIrO_3$ can be naively extracted by adopting the interpretation, though debated [34,35], of feature A in Fig. 2 as the excitation across the Mott gap [28]: we obtain $U \simeq 0.4$ eV which is consistent with the band gap of 0.34 eV deduced from resistivity measurements [18,20] and places $CaIrO_3$ in the scenario of Fig. 4(f).

In conclusion, we solve the controversy concerning the ground state of $CaIrO_3$ [14,18,19]: $CaIrO_3$ is *not* a $j_{\mathrm{eff}} = 1/2$ iridate. Indeed, we estimate the effective tetragonal crystal field splitting ($\Delta = -0.71$ eV) by inspecting the Ir L_3 edge RIXS response in the energy range relevant to spin-orbital excitations. To the best of our knowledge, this is the largest noncubic crystal field splitting reported for iridium oxides. Moreover, we show that experimental [14] and theoretical [18,19] results can be reconciled in view of the nontrivial dependence of the Ir L_2/L_3 RMXS intensity ratio on the magnetic moment direction [17] and we understand that the sign of magnetic interactions is unchanged with respect to the ideal $j_{\mathrm{eff}} = 1/2$ case because the even occupancy and the phase relation of the yx and zx orbitals is preserved. Finally, we clarify how the Mott insulating state survives in $CaIrO_3$ despite the severe departure from the $j_{\mathrm{eff}} = 1/2$ ground state, thus extending the physics of correlated iridates beyond model materials such as Sr_2IrO_4.

Enlightening discussions with G. Jackeli are kindly acknowledged. The experiment largely profited from the technical support and expertise of R. Verbeni and C. Henriquet. The work in Japan was partly supported by Grant-in-Aid for Scientific Research (B) (Grant No. 26287073).

*marco.moretti@esrf.fr

[1] B. J. Kim, H. Jin, S. J. Moon, J. Kim, B. G. Park, C. S. Leem, J. Yu, T. W. Noh, C. Kim, S. J. Oh, J. H. Park, V. Durairaj, G. Cao, and E. Rotenberg, Phys. Rev. Lett. **101**, 076402 (2008).
[2] S. J. Moon, H. Jin, K. W. Kim, W. S. Choi, Y. S. Lee, J. Yu, G. Cao, A. Sumi, H. Funakubo, C. Bernhard, and T. W. Noh, Phys. Rev. Lett. **101**, 226402 (2008).
[3] B. J. Kim, H. Ohsumi, T. Komesu, S. Sakai, T. Morita, H. Takagi, and T. Arima, Science **323**, 1329 (2009).
[4] V. M. Katukuri, H. Stoll, J. van den Brink, and L. Hozoi, Phys. Rev. B **85**, 220402 (2012).
[5] H. Zhang, K. Haule, and D. Vanderbilt, Phys. Rev. Lett. **111**, 246402 (2013).
[6] S. Boseggia, H. C. Walker, J. Vale, R. Springell, Z. Feng, R. S. Perry, M. Moretti Sala, H. M. Rønnow, S. P. Collins, and D. F. McMorrow, J. Phys. Condens. Matter **25**, 422202 (2013).
[7] M. Moretti Sala, M. Rossi, S. Boseggia, J. Akimitsu, N. B. Brookes, M. Isobe, M. Minola, H. Okabe, H. M. Ronnow, L. Simonelli, D. F. McMorrow, and G. Monaco, Phys. Rev. B **89**, 121101(R) (2014).
[8] S. Hirai, M. Welch, F. Aguado, and S. Redfern, Z. Kristallogr. **224**, 345 (2009).
[9] S. Boseggia, R. Springell, H. C. Walker, A. T. Boothroyd, D. Prabhakaran, D. Wermeille, L. Bouchenoire, S. P. Collins, and D. F. McMorrow, Phys. Rev. B **85**, 184432 (2012).
[10] S. Boseggia, R. Springell, H. C. Walker, A. T. Boothroyd, D. Prabhakaran, S. P. Collins, and D. F. McMorrow, J. Phys. Condens. Matter **24**, 312202 (2012).

[11] J. W. Kim, Y. Choi, J. Kim, J. F. Mitchell, G. Jackeli, M. Daghofer, J. van den Brink, G. Khaliullin, and B. J. Kim, Phys. Rev. Lett. **109**, 037204 (2012).
[12] S. Boseggia, R. Springell, H. C. Walker, H. M. Rønnow, C. Rüegg, H. Okabe, M. Isobe, R. S. Perry, S. P. Collins, and D. F. McMorrow, Phys. Rev. Lett. **110**, 117207 (2013).
[13] S. Calder, G.-X. Cao, S. Okamoto, J. W. Kim, V. R. Cooper, Z. Gai, B. C. Sales, M. D. Lumsden, D. Mandrus, and A. D. Christianson, Phys. Rev. B **89**, 081104(R) (2014).
[14] K. Ohgushi, J.-i. Yamaura, H. Ohsumi, K. Sugimoto, S. Takeshita, A. Tokuda, H. Takagi, M. Takata, and T.-h. Arima, Phys. Rev. Lett. **110**, 217212 (2013).
[15] L. C. Chapon and S. W. Lovesey, J. Phys. Condens. Matter **23**, 252201 (2011).
[16] D. Haskel, G. Fabbris, M. Zhernenkov, P. P. Kong, C. Q. Jin, G. Cao, and M. van Veenendaal, Phys. Rev. Lett. **109**, 027204 (2012).
[17] M. Moretti Sala, S. Boseggia, D. F. McMorrow, and G. Monaco, Phys. Rev. Lett. **112**, 026403 (2014).
[18] A. Subedi, Phys. Rev. B **85**, 020408 (2012).
[19] N. A. Bogdanov, V. M. Katukuri, H. Stoll, J. van den Brink, and L. Hozoi, Phys. Rev. B **85**, 235147 (2012).
[20] K. Ohgushi, H. Gotou, T. Yagi, Y. Kiuchi, F. Sakai, and Y. Ueda, Phys. Rev. B **74**, 241104 (2006).
[21] L. J. P. Ament, M. van Veenendaal, T. P. Devereaux, J. P. Hill, and J. van den Brink, Rev. Mod. Phys. **83**, 705 (2011).
[22] L. J. P. Ament, G. Khaliullin, and J. van den Brink, Phys. Rev. B **84**, 020403 (2011).
[23] J. Kim, D. Casa, M. H. Upton, T. Gog, Y.-J. Kim, J. F. Mitchell, M. van Veenendaal, M. Daghofer, J. van den Brink, G. Khaliullin, and B. J. Kim, Phys. Rev. Lett. **108**, 177003 (2012).
[24] A. Lupascu, J. P. Clancy, H. Gretarsson, Z. Nie, J. Nichols, J. Terzic, G. Cao, S. S. A. Seo, Z. Islam, M. H. Upton, J. Kim, A. H. Said, D. Casa, T. Gog, V. M. Katukuri, L. Hozoi, J. van den Brink, H. Stoll, and Y.-J. Kim, Phys. Rev. Lett. **112**, 147201 (2014).
[25] J. Kim, A. H. Said, D. Casa, M. H. Upton, T. Gog, M. Daghofer, G. Jackeli, J. van den Brink, G. Khaliullin, and B. J. Kim, Phys. Rev. Lett. **109**, 157402 (2012).
[26] X. Liu, V. M. Katukuri, L. Hozoi, W.-G. Yin, M. P. M. Dean, M. H. Upton, J. Kim, D. Casa, A. Said, T. Gog, T. F. Qi, G. Cao, A. M. Tsvelik, J. van den Brink, and J. P. Hill, Phys. Rev. Lett. **109**, 157401 (2012).
[27] L. Hozoi, H. Gretarsson, J. P. Clancy, B.-G. Jeon, B. Lee, K. H. Kim, V. Yushankhai, P. Fulde, Y.-J. Kim, and J. van den Brink, Phys. Rev. B **89**, 115111 (2014).
[28] H. Gretarsson, J. P. Clancy, X. Liu, J. P. Hill, E. Bozin, Y. Singh, S. Manni, P. Gegenwart, J. Kim, A. H. Said, D. Casa, T. Gog, M. H. Upton, H.-S. Kim, J. Yu, V. M. Katukuri, L. Hozoi, J. van den Brink, and Y.-J. Kim, Phys. Rev. Lett. **110**, 076402 (2013).
[29] See Supplemental Material at http://link.aps.org/supplemental/10.1103/PhysRevLett.112.176402 for details of the experimental setup, which includes Refs. [30,31].
[30] M. Moretti Sala, C. Henriquet, L. Simonelli, R. Verbeni, and G. Monaco, J. Electron Spectrosc. Relat. Phenom. **188**, 150 (2013).
[31] C. Ponchut, J. M. Rigal, J. Clément, E. Papillon, A. Homs, and S. Petitdemange, JINST **6**, C01069 (2011).
[32] K. Ishii, I. Jarrige, M. Yoshida, K. Ikeuchi, J. Mizuki, K. Ohashi, T. Takayama, J. Matsuno, and H. Takagi, Phys. Rev. B **83**, 115121 (2011).
[33] H. Gretarsson, J. P. Clancy, Y. Singh, P. Gegenwart, J. P. Hill, J. Kim, M. H. Upton, A. H. Said, D. Casa, T. Gog, and Y.-J. Kim, Phys. Rev. B **87**, 220407 (2013).
[34] K. Foyevtsova, H. O. Jeschke, I. I. Mazin, D. I. Khomskii, and R. Valentí, Phys. Rev. B **88**, 035107 (2013).
[35] B. H. Kim, G. Khaliullin, and B. I. Min, Phys. Rev. B **89**, 081109(R) (2014).
[36] G. Jackeli and G. Khaliullin, Phys. Rev. Lett. **102**, 017205 (2009).